Journal of Medicinal Chemistry

Article

pubs.acs.org/jmc

Structure−Activity and Structure−Property Relationship and Exploratory in Vivo Evaluation of the Nanomolar Keap1−Nrf2 Protein−Protein Interaction Inhibitor

Zheng-Yu Jiang,[†,‡] Li−Li Xu,[†,‡] Meng-Chen Lu,[†,‡] Zhi-Yun Chen,[†,‡] Zhen-Wei Yuan,[†,‡] Xiao-Li Xu,[†,‡,§] Xiao-Ke Guo,[†,‡,§] Xiao-Jin Zhang,[†,‡,∥] Hao-Peng Sun,*[,†,‡,§] and Qi-Dong You*[,†,‡]

[†]State Key Laboratory of Natural Medicines, China Pharmaceutical University, Nanjing 210009, China

[‡]Jiang Su Key Laboratory of Drug Design and Optimization, China Pharmaceutical University, Nanjing 210009, China

[§]Department of Medicinal Chemistry, School of Pharmacy, China Pharmaceutical University, Nanjing 210009, China

[∥]Department of Organic Chemistry, School of Science, China Pharmaceutical University, Nanjing 210009, China

Supporting Information

ABSTRACT: Directly disrupting the Keap1−Nrf2 protein−protein interaction (PPI) is an effective way to activate Nrf2. Using the potent Keap1−Nrf2 PPI inhibitor that was reported by our group, we conducted a preliminary investigation of the structure−activity and structure−property relationships of the ring systems to improve the drug-like properties. Compound **18e**, which bore *p*-acetamido substituents on the side chain phenyl rings, was the best choice for balancing PPI inhibition activity, physicochemical properties, and cellular Nrf2 activity. Cell-based experiments with **18e** showed that the Keap1−Nrf2 PPI inhibitor can activate Nrf2 and induce the expression of Nrf2 downstream proteins in an Nrf2-dependent manner. An exploratory in vivo experiment was carried out to further evaluate the anti-inflammatory effects of **18e** in a LPS-challenged mouse model. The primary results indicated that **18e** could reduce the level of circulating pro-inflammatory cytokines induced by LPS and relieve the inflammatory response.

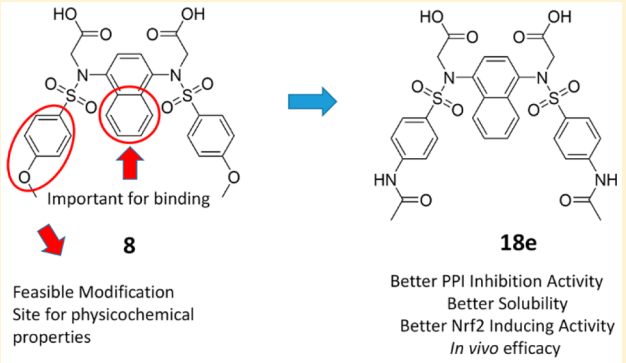

INTRODUCTION

Nrf2 (nuclear factor erythroid 2-related factor 2), a basic leucine zipper (bZIP) transcription factor, is the primary master of the inducible cell defense system. It can mediate the transcription of a battery of cytoprotective genes, including antioxidant proteins, phase I and II detoxification enzymes, transport proteins, proteasome subunits, chaperones, growth factors, and their receptors, as well as some transcription factors.[1−3] These cytoprotective genes all contain the enhancer sequence ARE (antioxidant response element, 5′-GTGACnnnGC-3′) in their promoter regulatory region, which is the binding target of Nrf2. Modulators regulating Nrf2 activity are of interest for their promising clinic applications in treating inflammatory diseases.[4−6]

Nrf2 is mainly regulated by Kelch-like ECH associated protein 1 (Keap1), which is an adaptor component of CUL3-based E3 ligase (Figure 1). Keap1 can mediate the ubiquitination of Nrf2, which leads to its subsequent degradation by proteasomes. The rapid turnover of Nrf2 can sustain the low activity of Nrf2 under normal conditions. Under stressed conditions, the cysteine residues in Keap1 can be covalently modified by ROS or electrophiles, which can lead to the dissociation of the Cul3−Keap1−Nrf2 complex and inhibit the Keap1-dependent depression of Nrf2. Consequently, Nrf2 accumulates and Keap1−Nrf2−ARE pathway is activated. The traditional electrophilic Nrf2 activators can mimic this endogenous process of Nrf2 activation. The most successful Nrf2 activator, dimethyl fumarate (DMF), has been approved by the FDA for the treatment of patients with relapsing forms of multiple sclerosis (MS) as a new first-line oral drug. The phase 3 study of another promising candidate, CDDO-Me, was terminated for safety reasons. The molecular mechanism of these activators is covalent binding to the thiol of the cysteine.[7] Thus, the risk of "off-target" effects may be associated with these Nrf2 activators due to their potential to react with other cysteine-containing proteins and enzymes.[5]

Recently, directly and competitively interrupting the Keap1−Nrf2 protein−protein interaction has been shown to be an alternative method for enhancing Nrf2 activity. Peptides that mimic Nrf2 can disrupt the Keap−Nrf2 interaction.[8] Additionally, the ETGE motif of Nrf2 was conjugated to a cell-

Received: February 1, 2015

DOI: 10.1021/acs.jmedchem.5b00185
J. Med. Chem. XXXX, XXX, XXX−XXX

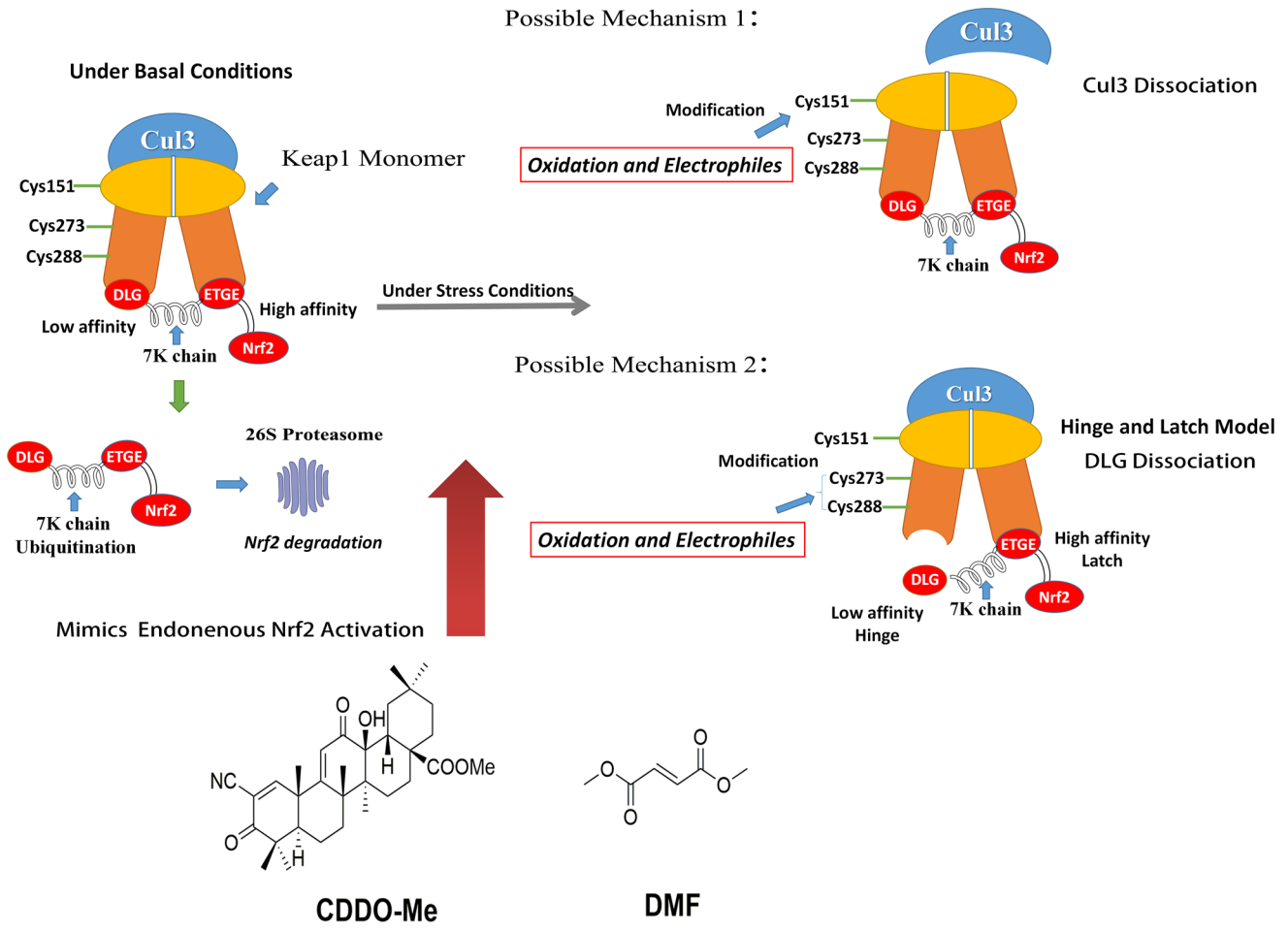

Figure 1. Keap1−Nrf2 regulation model and mechanism of action of electrophilic Nrf2 activators.

penetrating peptide, which is a trans-activating transcriptional activator (TAT) peptide derived from HIV, and this conjugation resulted in a fused peptide. It was shown to activate Nrf2 and its downstream target gene, heme-oxygenase-1 (HO-1), in a dose-dependent manner in intact human THP-1 monocytes.[9] However, inhibition with small molecules is a more attractive proposal because of the pharmacological advantages of small molecule drugs including enhanced stability and oral bioavailability.[10] Inspired by the successful development of peptide inhibitors, two high throughput screenings for small molecular PPI inhibitors of Nrf2−Keap1 have been reported by different groups. Fluorescence polarization (FP) based screening of the MLPCN library gave compound **1**, with an IC_{50} of 3 μM.[11] The detailed binding mode and structure−activity relationship (SAR) of compound **1** has also been investigated.[12] Homogeneous confocal fluorescence anisotropy assay (two-dimensional fluorescence intensity distribution analysis, 2D-FIDA) screening of an Evotec Lead Discovery library screened out compounds **2** and **3**, with an EC_{50} of 118 and 2.7 μM, respectively.[13] In additional to high-throughput screening, different groups have used a virtual screening method to identify novel Keap1−Nrf2 PPI inhibitors. Our group used a receptor−ligand binding model of Nrf2−Keap1 to carry out a hierarchical structure-based virtual screening. We successfully discovered compound **4**, which can effectively disrupt the Nrf2−Keap1 interaction with an in vitro EC_{50} of 9.80 μM in the FP assay.[14] Compound **4** can enhance Nrf2 transcriptional activity in the cellular ARE-luciferase reporter assay in a dose-dependent manner. In another study,[15] the docking method known as Schrodinger's Glide was used to discover three classes of novel inhibitors that are capable of disrupting Keap1−Nrf2 (compound **5**, **6**, and **7**). The most potent compound had a K_{D2} of 2.9 μM in the fluorescence anisotropy assay. These active hits had a Keap1 binding IC_{50} in the sub-μM range, which is much less potent than the natural substrate. Thus, the potency of these compounds on Nrf2−ARE activation was limited. Recently, on the basis of a molecular binding determinants analysis of Keap1, we successfully designed and characterized the most potent PPI inhibitor of Keap1−Nrf2, compound **8**, with a K_D value for binding to Keap1 in the single-digit nanomolar (Figure 2).[16] Compound **8**, containing two aliphatic carboxylic acid side chains, can mimic Glu79 and Glu82 in the Nrf2 ETGE motif. This result suggests that the proper occupation of the polar subpockets, P1 and P2, should be addressed in the rational design of the PPI inhibitors of Keap1. Until now, the direct PPI inhibitors of Keap1−Nrf2 have been effective only at the protein and cellular level. Whether these inhibitors can exert their effects in vivo has not been validated.

In this study, on the basis of the potent inhibitor **8** discovered by our group, the structure−activity and structure−property relationships were investigated. The optimized compound **18e** showed a similar inhibition activity in the in vitro FP assay, but significant advantages in physicochemical properties, especially solubility. The cell-based ARE luciferase reporter assay also showed that **18e** has a better Nrf2-inducing

DOI: 10.1021/acs.jmedchem.5b00185
J. Med. Chem. XXXX, XXX, XXX−XXX

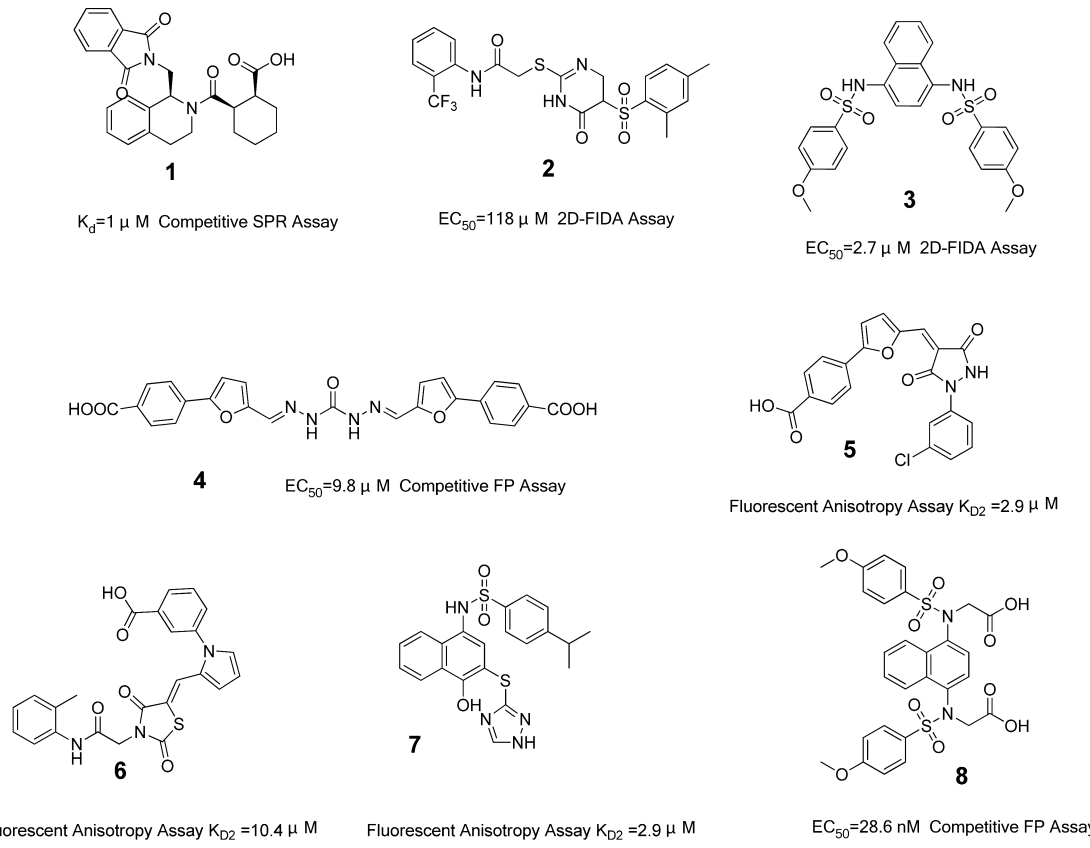

Figure 2. Chemical structures of Keap1−Nrf2 PPI inhibitors.

Scheme 1. Synthesis of Compounds with a Phenyl Ring As the Scaffold[a]

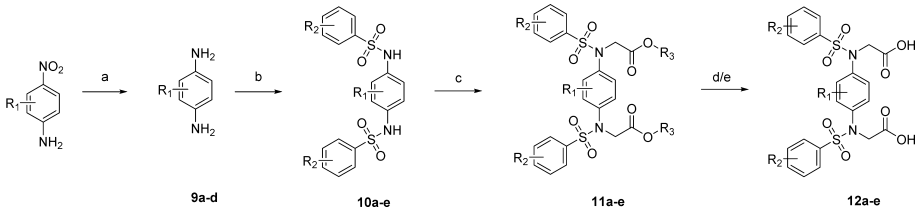

[a]Reagents and conditions: (a) Pd/C, H_2, rt, 4 h; (b) substituted benzenesulfonyl chloride, THF, pyridine, 40 °C, 4 h, 54%; (c) DMF, K_2CO_3, ethyl bromoacetate, rt, 3 h, 74%; (d) R_3 = ethyl, NaOH, MeOH, H_2O, 65 °C, 2 h, 71%; (e) R_3 = methyl, LiOH, MeOH, H_2O, RT, overnight. The yields were shown using **12a** as an example.

activity. This compound was subsequently used for the exploratory in vivo evaluation of the anti-inflammatory effects in the LPS (lipopolysaccharide) challenge model. Pretreatments with **18e** markedly changed the overall response profiles induced by LPS, especially for the circulating pro-inflammatory cytokines. These results suggested that Keap1−Nrf2 PPI inhibitor pretreatment can confer protective effects against LPS challenge and relieve the overall inflammatory response. This result encourages the further evaluation of the therapeutic effects on inflammatory diseases.

RESULTS AND DISCUSSIONS

The Core Naphthalene Ring Is the Key Feature for Nrf2−Keap1 PPI Inhibitor. Our previously reported Nrf2−Keap1 PPI inhibitor **8** had a good Keap1 binding affinity (9.91 nM) and displayed potent inhibition effects in the in vitro Keap1−Nrf2 FP assay (28.6 nM). It can also significantly elevate Nrf2 activity in cell-based experiments. With the aim of identifying a Keap1−Nrf2 inhibitor active in vivo, we continued to evaluate the physicochemical properties of **8** in the present study. The results showed that **8** is of low solubility (388 μg/mL), which may restrict the accurate assessment of in vivo effects. Thus, the subsequent research program mainly focused on the investigation of the SAR and the structure−property relationship (SPR) of **8**.

According to previous research, the *N*-acetic acid substituted sulfonamide groups of **8** play an important role in Keap1 binding. These groups can form multiple polar interactions, including hydrogen bonds and salt bridges with polar residues in the P1 and P2 subpockets of Keap1. Thus, we mainly focused on the aromatic rings of **8** to improve its physicochemical properties.

Our initial task was to evaluate the requirement of naphthalene for activity because the planarity and hydrophobicity of the core naphthalene ring may restrict the solubility. Simplifying the naphthalene to a phenyl ring resulted in **12a** (Scheme 1). The FP results showed that such simplification led to a dramatic decrease in activity, which

DOI: 10.1021/acs.jmedchem.5b00185
J. Med. Chem. XXXX, XXX, XXX−XXX

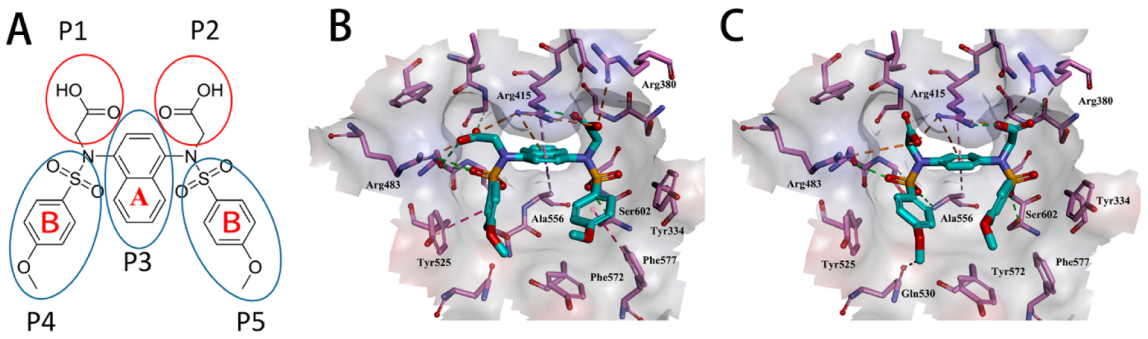

Figure 3. Docking study of the binding mode differences between **8** and **12a**. (A) Structure analysis of **8**. (B,C) Binding mode of **8** and **12a** from docking. The hydrogen bonds are represented as green dashed lines, and the electrostatic interactions are represented as yellow dashed lines. The carbon atoms of the ligands and Keap1 residues are colored cyan and purple, respectively.

was unacceptable for PPI inhibition. To fully confirm this result, **12b** with 4-methyl substituents was synthesized, and the experimental results were similar to those obtained for **12a**.

We further investigated the binding mode differences between **8** and **12a** using a docking method. As shown in Figure 3, the two compounds did not show great differences in binding to Keap1. The interacting pattern analysis gave two possible reasons for the decrease in activity: one possibility is that the phenyl ring replacement of the naphthalene reduced the hydrophobic interactions inner the subpocket P3. Ring B of the naphthalene can form hydrophobic interactions with the side carbon chain of Arg415 and the side chain of Ala556. The other possibility could be that the removal of one phenyl ring reduced the π system and the polarizability of the aromatic ring. It may weaken the cation−π interaction between the guanidyl group in Arg415 and the core structure of the ligand. Therefore, **12a** was chosen as the template and the hydrophobic substituents were added to the core phenyl ring to investigate whether the complement of the hydrophobic interactions could compensate for the decrease in activity (**12c**−**12e**). Only **12e** with 2-methoxyl substituents showed a slight improvement in activity. These results indicated that the aliphatic hydrophobic groups cannot replace the core naphthalene ring. The planar aromatic ring with an extended π system is the key pharmacophore of the Keap1−Nrf2 PPI inhibitor, which should be retained for activity.

Substituent Transformation on the Side Chain Phenyl Ring Is Tolerable for Keap1−Nrf2 PPI Inhibition Activity. Considering that the two *N*-acetic acid substituted sulfonamide groups play an important role in Keap1 binding,[17] the substituents on the phenyl groups (ring B) of **8** were chosen as the next optimization sites. First, we compared the substituent position effects of the core naphthalene. The 1,5-substituted analogue, **15**, was synthesized. The FP experiment gave a negative result (IC_{50} = 1.86 μM), indicating the necessity of the 1,4-substitued core naphthalene (Table 1).

Then, we systematically evaluated the effects of different substituents on PPI inhibition activity. Generally, ring B can tolerate a variety of substituents (Table 2). The electron-withdrawing substituents are not preferred for Keap1−Nrf2 PPI inhibition activity, whereas the electron-donating groups can exhibit better performance. Among the electron-donating groups, the substituents with steric bulk are not appropriate. Both **18f** with 4-tertiary-butyl substitutes and **18j** containing naphthalene sulfonyl fragments are less active (Scheme 2). The 2,4,6-trimethyl substituted compound **18g** showed a dramatic decrease in activity, indicating that the ortho position was

Table 1. IC_{50} of Compounds Bearing the Phenyl Ring Scaffold for the Inhibition of Keap1 Kelch Domain−Nrf2 ETGE Interaction[a]

compd	R1	R2	IC_{50} (nM) 95% CI
8			30.8
			27.6−34.4
12a	H	4-OCH_3	1448
			1325−1671
12b	H	4-CH_3	966
			900−1036
12c	2-CH_3	4-OCH_3	1666
			1262−2620
12d	2,5-CH_3	4-OCH_3	10.17[a]
			8.46−12.24[a]
12e	2-OCH_3	4-OCH_3	602
			477−759

[a]The unit is μM.

sensitive to steric hindrance. The potency of 3-methoxyl substituted compound **18l** was lower, thus further confirming that the electron-donating groups were preferable in the para position. The *p*-methyl substituent was slightly more potent than *p*-methoxyl. Interestingly, the phenyl ring without any substituent also exhibited high potency, which indicated that the electron-donating group was not the determinant for activity. Although the overall performance of electron-withdrawing was less potent, the *p*-acetamido substitutes can give excellent performance.

Substituent Transformation on the Ring Has Dramatic Effects on Solubility and Cellular Nrf2 Inducing Activity. After the SAR study of the substitutes on ring B, the physicochemical properties were determined for further analysis of SPR. Unlike the SAR results, the electron-withdrawing and halogen substituents showed better results than the electron-donating groups. The electron-donating groups, especially those hydrophobic groups without polar atoms, decreased the solubility significantly. The electron-withdrawing substituents can improve the solubility. Halogen substituents had dramatic differences in solubility: F- and Cl- were beneficial for solubility, whereas Br- was disadvantageous. Attractively, **18e** with the *p*-acetamido substitutes also showed advantages in solubility.

The cellular activities of these compounds were further evaluated using the ARE-luciferase reporter assay in HepG2−ARE−C8 cells. **18e** with *p*-acetamido substitutes, which is optimal in both PPI inhibition activity and solubility, gave the

DOI: 10.1021/acs.jmedchem.5b00185
J. Med. Chem. XXXX, XXX, XXX−XXX

Table 2. IC_{50}, Physicochemical Properties, and ARE Induction Fold Results of the Compounds Containing Various Substituents on Ring B[a]

compd	R_1	IC_{50} (nM) 95% CI	solubility	log *D*, pH 7.4	induction fold 0.1 μM	1 μM	5 μM
8	4-OCH_3	30.8 27.6−34.4	388 μg/mL	1.71	1.79 ± 0.43	3.49 ± 0.09	5.93 ± 1.27
18a	4-CH_3	18.1 15.0−21.8	248 μg/mL	0.93	1.49 ± 0.21	3.19 ± 0.24	5.51 ± 0.18
18b	4-F	54.3 49.9−59.1	3.8 mg/mL	1.16	1.42 ± 0.14	1.79 ± 0.17	3.19 ± 0.40
18c	4-Cl	42.3 34.8−51.4	1.2 mg/mL	2.11	1.66 ± 0.07	1.99 ± 0.09	2.52 ± 0.91
18d	4-Br	36.5 29.7−44.8	5.7 μg/mL	4.29	1.83 ± 0.55	2.16 ± 0.48	2.40 ± 0.10
18e	4-acetamido	14.4 12.4−16.7	5.0 mg/mL	1.02	2.81 ± 0.67	6.69 ± 1.56	10.61 ± 1.21
18f	4-$C(CH_3)_3$	50.2 42.8−58.9	1.6 μg/mL	5.2	1.19 ± 0.15	1.51 ± 0.23	2.18 ± 0.31
18g	2,4,6-trimethyl	979 672−1425	20.0 μg/mL	3.44	1.51 ± 0.19	1.67 ± 0.14	1.99 ± 0.08
18h	H	34.3 30.3−38.9	183 μg/mL	0.45	1.47 ± 0.08	1.67 ± 0.14	6.25 ± 0.82
18i	4-OCF_3	179 144−222	12.3 μg/mL	0.93	1.76 ± 0.11	1.89 ± 0.55	1.45 ± 0.11
18j	5,6-C_4H_4	47.4 37.9−59.2	5.0 μg/mL	3.9	1.92 ± 0.02	2.57 ± 0.12	4.46 ± 0.49
18k	4-CF_3	122 98.1−151	12.3 μg/mL	2.81	1.60 ± 0.02	1.69 ± 0.01	2.03 ± 0.40
18l	3-OCH_3	66.1 55.9−78.3	16.0 μg/mL	0.89	1.88 ± 0.66	2.22 ± 0.02	3.99 ± 1.02
18m	4-CN	118 84.0−165	1.1 mg/mL	0.65	1.59 ± 0.50	1.40 ± 0.10	2.79 ± 0.19
18n	4-*n*-butyl	42.2 37.5−47.4	6.0 ng/mL	1.89	1.81 ± 0.03	1.77 ± 0.43	2.58 ± 0.28

[a]Induction fold was shown as a ratio to the DMSO control, and data are presented as mean ± SEM of three separate experiments.

Scheme 2. Synthesis of Compounds with Various Substitutes on Ring B[a]

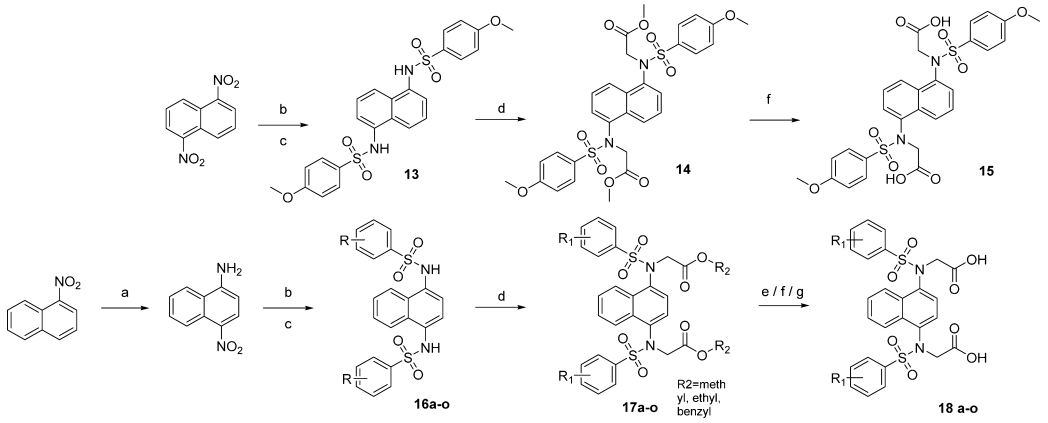

[a]Reagents and conditions: (a) $NH_2OH{\cdot}HCl$, 95% ethanol, MeOH, 60 °C, 2 h; (b) Pd/C, H_2, rt, 4 h; (c) 4-methoxybenzenesulfonyl chloride, toluene, pyridine, 100 °C, 2 h, 67%; (d) DMF, K_2CO_3, ethyl bromoacetate, rt, 3 h, 58%; (e) R_2 = ethyl, NaOH, MeOH, H_2O, 65°, 2 h, 64%; (f) R_2 = methyl, LiOH, MeOH, H_2O, RT, overnight; (g) R_2 = benzyl, Pd/C, H_2, 40 °C, 6 h. The yields were shown using **18a** as an example.

best performance among these compounds. Therefore, it was chosen for additional cell-based and in vivo evaluation. Although the electron-donating hydrophobic substituted analogues (**18f** and **18n**) exhibited potent PPI inhibition activity, their low solubility restricts their cellular potency in Nrf2−ARE activation. Only these compounds with proper in vitro Keap1−Nrf2 PPI inhibition activity and acceptable solubility simultaneously can be potent Nrf2−ARE activators. The apparent shortcoming on either sides would abolish the cellular activity. We also further evaluated the ligand efficiency (LE), ligand efficiency dependent lipophilicity (LELP), and lipophilic efficiency (LipE) of these compounds (detailed

DOI: 10.1021/acs.jmedchem.5b00185
J. Med. Chem. XXXX, XXX, XXX−XXX

results can be found in the Supporting Information). Overall, the LE did not correlate with the cellular activity, whereas LELP and LipE were closely related to the Nrf2−ARE inducing activity. The compounds with low LELP and high LipE were more potent in the cellular assay. These results indicated that affinity changes depend on the molecule that interact directly with the protein, and enthalpy-driven binding profiles[18] are more advantageous for Nrf2−ARE inducing activity, which can satisfy the expectation for the molecular optimization of Keap1−Nrf2 PPI inhibitor.

Keap1−Nrf2 PPI Inhibitor Can Elevate the Protein Level of Nrf2-Regulated Genes. We further examined the concentration-dependent effect of **18e** on the protein level of Nrf2-driven genes including heme oxygenase-1 (HO-1), NAD(P)H/quinone oxidoreductase (NQO1), and γ-glutamyl-cysteine synthetase (γ-GCS). As shown in Figure 4A, **18e** can

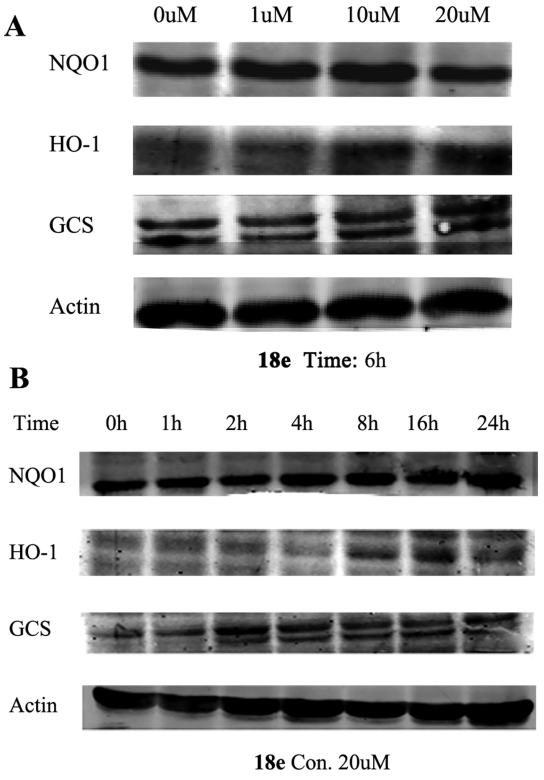

Figure 4. (A) Dose-dependent increase of Nrf2-regulated proteins after treatment with compound **18e**. HCT116 cells were treated with **18e** at different concentrations (1−20 μM). HO-1, NQO1, and γ-GCS were determined using β-actin as the loading control after 6 h of treatment with **18e**. (B) Time course study of Nrf2-regulated proteins after treatment with **18e** (20 μM) at various time points. NQO1, HO-1, and γ-GCS were determined using β-actin as loading control.

dose dependently increase the protein level of HO-1 and γ-GCS in the HCT116 cells. The elevation of NQO-1 was not so obvious. The basal level of NQO-1 in HCT116 cells was high, which was consistent with previously published results using HCT116 cells.[16] For the time course studies, the compound maximized the expression of HO-1, NQO1, and GCS at 16−24 h, respectively (Figure 4B). The result was consistent with the result for **8** reported previously and showed a distinct behavior toward electrophilic Nrf2 activators.[14,16] These data further confirmed that **18e** can elevate the downstream proteins of Nrf2 at the cellular level.

The Elevation of the Nrf2-Regulated Enzymes Induced by 18e Depends on Nrf2. An Nrf2 knockdown strategy was used to further confirm that **18e** activates Nrf2 downstream genes through Nrf2. HCT116 cells were treated with Nrf2 siRNA, **18e**, or Nrf2 siRNA plus **18e**. The untreated HCT116 cells were used as the blank control. Nrf2 siRNA induced a significant inhibition of the mRNA level of Nrf2 together with its transcription target genes NQO1, GCLM, and HO-1 (Figure 5). The induction of HO-1, GCLM, and NQO-1

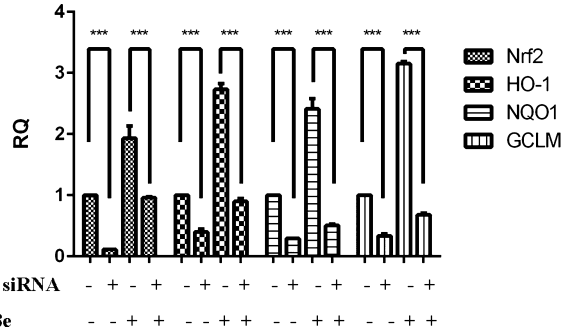

Figure 5. Expression of Nrf2 and Nrf2-regulated genes after treatment with Nrf2 siRNA and **18e**. HCT116 cells were treated with Nrf2 siRNA (50 nM), **18e** (20 μM), or Nrf2 siRNA (50 nM) plus **18e** (20 μM). The expression of Nrf2, GCLM, NQO-1, and HO-1 genes were quantified using qRT-PCR. The values shown are the mean ± SD (n = 3). ***p < 0.001.

by **18e** sharply decreased as a result of Nrf2 knockdown. The addition of compound **18e** into the Nrf2 siRNA group only up-regulated these genes to the normal level, similar to the blank control. This result is consistent with the well-known Nrf2 activator sulforaphane.[19] These results indicated that **18e** can elevate the expression of Nrf2 downstream genes in an Nrf2-dependent manner.

Keap1−Nrf2 PPI Inhibitor Can Relieve Mouse Inflammatory Responses Induced by LPS Challenge. After the validation of the potency of **18e** in the cell-based experiments, the in vivo anti-inflammatory effects of **18e** in the context of the LPS challenge was evaluated. LPS can lead to both MyD88-dependent early phase NF-κB transcription of pro-inflammatory cytokines, such as TNF-α, and IL-6 and MyD88-independent, late phase NF-κB transcription of IFN-β.[20] It can also promote inflammation by inducing the production of reactive oxygen species.[21] It is commonly used to induce the inflammatory response, which has been successfully used in the Nrf2 activator.[22] The production of pro-inflammatory cytokines is a critical marker for inflammation, and these inflammatory cytokines are an important cause of the inflammatory damage. Thus, the circulating inflammatory cytokines were chosen as the main marker for monitoring anti-inflammatory effects. C57BL/6 mice were pretreated with **18e** (low dose 10 mg/kg/day or high dose 80 mg/kg/day) for 3 days (day −3, −2, −1) and then challenged with LPS (300 μg IP) 24 h after the last dose of compound (day 0). The untreated group received saline (day −3, −2, −1) and then the LPS challenge (day 0). The blank group only received saline during the experiment. Dexamethasone, the widely used steroid anti-inflammatory drug, was used as positive control (10 mg/kg/day, the same procedure as **18e**). Sera were collected from all groups 5 h post-LPS challenge. The level of the cytokines in sera was measured using ELISA.

DOI: 10.1021/acs.jmedchem.5b00185
J. Med. Chem. XXXX, XXX, XXX−XXX

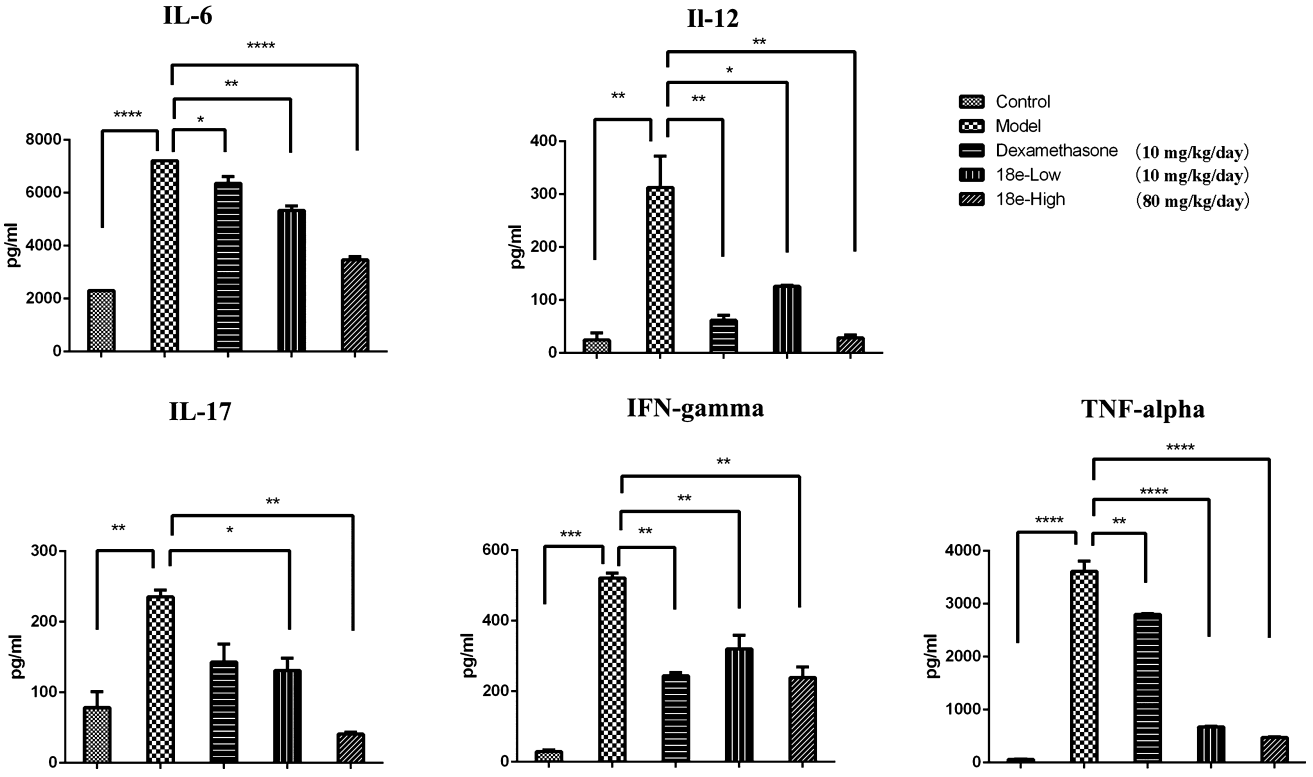

Figure 6. Quantification of various inflammatory cytokines, including IL-6, Il-12, IL-17, TNF-α, and IFN-γ, in the serum of C57BL/6 female mice after 5 h of LPS challenge. Dexamethasone (10 mg/kg) was used as the positive control. The data were shown as the mean ± SEM, *p < 0.05, **p < 0.01, ***p < 0.001, ****p < 0.0001, indicating the statistically significant difference from the untreated blank control group.

During the pretreatment of **18e**, no acute toxicity was observed and the body weights of the mice did not show significant changes (the detailed body weight data can be found in Supporting Information). As shown in Figure 6, both high dose and low dose compound **18e** can significantly and dose dependently reduce the levels of pro-inflammatory cytokines, including TNF-α and IFN-γ, as well as IL-6, IL-12, and IL-17, relative to LPS-challenged mice. Furthermore, **18e** had a more potent inhibitory activity against the production of IL-6, IL-17, and IFN-γ and comparable effects on IL-12 and TNF-α at the same concentration as the positive control dexamethasone (10 mg/kg/day). In general, these results suggested that **18e** pretreatment can reduce inflammatory cytokines and confer protection against LPS challenge. Thus, **18e** potentially possesses promising anti-inflammatory effects in vivo and should be further evaluated in LPS-mediated inflammatory disease models.

CONCLUSIONS

The Keap1−Nrf2−ARE pathway protects humans from chemical and oxidative insults by regulating the expression of various cytoprotective proteins. It plays an important role in the homeostatic regulation of the microenvironment. The dysregulation of the microenvironment, for example, an elevated oxidative state, is closely related to inflammatory disease. The development of anti-inflammatory agents has not made much progress in recent years. Nrf2 activation is an innovative strategy to treat inflammatory diseases through enhancing the innate defense mechanism.

On the basis of the potent Keap1−Nrf2 PPI inhibitor reported by our group previously, we investigated the structure−activity and structure−property relationships of the ring systems to improve the physicochemical properties, especially the solubility. The key structural features for Keap1 binding were retained, and the feasible optimization sites on the side chain phenyl ring were identified. We systematically evaluated the effects of different substituents on PPI inhibition activity, physicochemical properties, and cellular Nrf2 activity. **18e** with *p*-acetamido substituents was the best choice for balancing all of these aspects and was used for further investigations. Cell-based experiments using **18e** showed that the Keap1−Nrf2 PPI inhibitor can activate Nrf2 and induce the expression of Nrf2 downstream protein in an Nrf2-dependent manner. Encouraged by these results, an exploratory in vivo experiment was carried out to further confirm the anti-inflammatory effects of **18e** in the LPS-challenged mouse model. The primary results indicated that **18e** can reduce the circulating pro-inflammatory cytokines induced by LPS and relieve the inflammatory responses. This pioneering work advances the target validation of Keap1−Nrf2 PPI using small molecular agents.

MATERIALS AND METHODS

1. Chemistry. Reactions were monitored by thin-layer chromatography (TLC) on 0.25 mm silica gel plates (GF254) and visualized under UV light. Melting points were determined with a Melt-Temp II apparatus. The ^{1}H NMR and ^{13}C NMR spectra were measured on a Bruker AV-300 instrument using deuterated solvents with tetramethylsilane (TMS) as the internal standard. ESI-mass and high-resolution mass spectra (HRMS) were recorded on a Water Q-Tof micro mass spectrometer. The purity (≥95%) of the compounds was verified by HPLC performed on an Agilent C18 (4.6 mm × 150 mm, 3.5 μm) column using a mixture of solvent methanol/water 70:30 with 1‰ TFA at the flow rate of 0.5 mL/min and peak detection at 254 nm.

DOI: 10.1021/acs.jmedchem.5b00185
J. Med. Chem. XXXX, XXX, XXX−XXX

Target compounds **12a−e** were synthesized using similar procedures. The detailed procedures for the synthesis of **12a** are listed as an example; the others can be found in the Supporting Information.

*N,N′-(1,4-Phenylene)bis(4-methoxybenzenesulfonamide) (**10a**).* 4-Methoxybenzenesulfonyl chloride (3.75 g, 22 mmol) and pyridine (2.37 g, 30 mmol) was added to the solution of THF (20 mL) and 1,4-diaminobenzene (1.08 g, 10 mmol). The reaction mixture was stirred at 40 °C for 2 h. After the completion of the reaction monitored by TLC, the solvent was removed and 20 mL of 1 M hydrochloric acid was added, resulting in a lot of precipitation. After filtration, the solid was collected and washed with water. Recrystallization from 95% ethanol gave the white solid, yield 54%; mp 225−227 °C. ^{1}H NMR (300 MHz, DMSO, δ) 9.90 (s, 2H), 7.58−7.51 (m, 4H), 7.01−6.97 (m, 4H), 6.94−6.84 (m, 4H), 3.74 (s, 6H). HRMS (ESI): found 471.0687 ($C_{20}H_{20}N_2NaO_6S_2$, $[M + Na]^+$, requires 471.0655).

*Diethyl 2,2′-(1,4-Phenylenebis(((4-methoxyphenyl)sulfonyl)-azanediyl))diacetate (**11a**).* To a solution of **10a** (896 mg, 2 mmol) in DMF (5 mL) was added K_2CO_3 (830 mg, 6 mmol) followed by ethyl bromoacetate (836 mg, 5 mmol). After 3 h stirring at room temperature, the reaction mixture was then diluted in 30 mL of water and quenched with 2 M hydrochloric acid to pH 5. The crude product was obtained through filtration. Recrystallization from ethyl acetate/*n*-hexane gave the **11a** as a light-pink solid, yield 74%; mp 139−141 °C. ^{1}H NMR (300 MHz, DMSO, δ) 7.55 (d, 4H, J = 8.82 Hz), 7.11−6.99 (m, 8H), 4.46 (s, 4H), 4.06 (q, 4H, J = 7.08 Hz), 3.85 (s, 6H), 1.11(t, 6H, J = 7.08 Hz). HRMS (ESI): found 643.1408 ($C_{28}H_{32}N_2NaO_{10}S_2$, $[M + Na]^+$, requires 643.1391).

*2,2′-(1,4-Phenylenebis(((4-methoxyphenyl)sulfonyl)azanediyl))-diacetic Acid (**12a**).* To a solution of NaOH (2 g) in MeOH/H_2O (10/10 mL) was added **11a** (545 mg, 1 mmol). The reaction mixture was heated in an oil bath maintained at 65 °C for 2 h, then quenched with 2 M hydrochloric acid to pH 2 and diluted with 75 mL water. Precipitate removed by filtration and washed with 5 × 10 mL water, then dried overnight in a vacuum desiccator, yielding **12a** as a white solid, yield 71%; mp 232−234 °C. ^{1}H NMR (300 MHz, DMSO, δ) 12.89 (br, 2H), 7.53 (d, 4H, J = 8.91 Hz), 7.14−7.04 (m, 8H), 4.36 (s, 4H), 3.84 (s, 6H). ^{13}C NMR (75 MHz, DMSO, δ) 169.870, 162.667, 138.552, 129.647, 129.433, 127.674, 114.249, 55.652, 51.659. HRMS (ESI): found 587.0774 ($C_{24}H_{24}N_2NaO_{10}S_2$, $[M + Na]^+$, requires 587.0765). HPLC (70:30 methanol:water with 1‰ TFA): t_R = 5.1 min, 99.3%.

*2,2′-(1,4-Phenylenebis(tosylazanediyl))diacetic Acid (**12b**).* Light-pink solid, yield 68%; mp 222−224 °C. ^{1}H NMR (300 MHz, DMSO, δ) 7.47 (d, 4H, J = 7.92 Hz), 7.35 (d, 4H, J = 7.50 Hz), 7.07 (s, 4H), 4.33 (s, 4H), 2.38 (s, 6H). ^{13}C NMR (75 MHz, DMSO, δ) 169.711, 143.667, 140.182, 135.209, 129.604, 129.193, 127.211, 126.760, 126.027, 51.770, 20.992. HRMS (ESI): found 550.1333 ($C_{24}H_{28}N_3O_8S_2$, $[M + NH_4]^+$, requires 550.1312). HPLC (70:30 methanol:water with 1‰ TFA): t_R = 6.8 min, 96.2%.

*2,2′-((2-Methyl-1,4-phenylene)bis(((4-methoxyphenyl)sulfonyl)-azanediyl))diacetic Acid (**12c**).* To a solution of LiOH (2 g) in MeOH/H_2O (15/5 mL) was added **11c** (606 mg, 1 mmol). The reaction mixture was stirring at room temperature overnight, then quenched with 2 M hydrochloric acid to pH 2 and diluted with 50 mL of water. Precipitate removed by filtration and washed with 5 × 10 mL water, then dried overnight in a vacuum desiccator, yielding **12c** as a white solid, yield 73%; mp 231−232 °C. ^{1}H NMR (300 MHz, DMSO, δ) 12.86 (s, 2H), 7.59−7.51 (m, 4H), 7.10−7.07 (m, 5H), 6.82−6.79 (m, 2H), 4.37 (s, 2H), 4.22 (s, 2H), 3.85 (s, 6H), 2.17 (s, 3H). ^{13}C NMR (75 MHz, DMSO, δ) 169.862, 162.707, 139.609, 137.233, 129.794, 129.655, 129.517, 124.511, 114.229, 55.672, 55.246, 51.644, 17.949. HRMS (ESI): found 601.0914 ($C_{25}H_{26}N_2NaO_{10}S_2$, $[M + Na]^+$, requires 601.0921). HPLC (70:30 methanol:water with 1‰ TFA): t_R = 5.4 min, 99.0%.

*2,2′-((2,5-Dimethyl-1,4-phenylene)bis(((4-methoxyphenyl)-sulfonyl)azanediyl))diacetic Acid (**12d**).* The same procedure as **12c**, yield 81%; mp 253−255 °C. ^{1}H NMR (300 MHz, DMSO, δ) 12.80 (s, 2H), 7.55 (d, 4H, J = 8.58 Hz), 7.10 (d, 4H, J = 8.46 Hz), 6.77 (s, 2H), 4.20 (s, 4H), 3.86 (s, 6H), 2.02 (s, 6H). ^{13}C NMR (75 MHz, DMSO, δ) 169.876, 162.728, 138.040, 136.451, 131.634, 129.850, 129.712, 114.154, 55.673, 52.164, 17.304. HRMS (ESI): found 615.1066 ($C_{26}H_{28}N_2NaO_{10}S_2$, $[M + Na]^+$, requires 615.1078). HPLC (70:30 methanol:water with 1‰ TFA): t_R = 5.9 min, 98.3%.

*2,2′-((2-Methoxy-1,4-phenylene)bis(((4-methoxyphenyl)sulfonyl)-azanediyl))diacetic Acid (**12e**).* The same procedure as **12c**, yield 81%; mp 247−248 °C. ^{1}H NMR (300 MHz, DMSO, δ) 12.78 (br, 2H), 7.60 (d, 2H, J = 8.43 Hz), 7.48 (d, 2H, J = 8.67 Hz), 7.31 (d,1H, J = 8.25 Hz), 7.10−7.02 (m,4H), 6.80 (d, 1H, J = 8.28 Hz), 6.59 (s, 1H), 4.40 (s, 2H), 4.19 (s, 2H), 3.84 (s, 6H), 3.17 (s, 3H). ^{13}C NMR (75 MHz, DMSO, δ) 170.322, 169.983, 162.759, 162.466, 155.316, 141.011, 133.114, 131.138, 129.735, 129.621, 129.165, 125.327, 119.149, 114.239, 113.832, 110.920, 55.681, 55.631, 55.164, 51.752, 50.640. HRMS (ESI): found 612.1309 ($C_{25}H_{30}N_3O_{11}S_2$, $[M + NH_4]^+$, requires 612.1316). HPLC (70:30 methanol:water with 1‰ TFA): t_R= 5.1 min, 95.4%.

Target compounds **18a−o** were synthesized according to the previous reported method[16] for synthesis of **8**. Detailed procedures of **18a** are listed as an example; the others can be found in the Supporting Information.

*N,N′-(Naphthalene-1,4-diyl)bis(4-methylbenzenesulfonamide) (**16a**).* To a solution of 4-nitronaphthalen-1-amine (1.81 g, 10 mmol) in THF was added Pd/C. The reaction mixture was stirred under hydrogen for 4 h. The solution was filtered to remove the catalyst. The filtrate was concentrated under reduced pressure to give the light-yellow oil. The crude product, naphthalene-1,4-diamine, was used without further purification. 4-Methylbenzenesulfonyl chloride (4.54g, 22 mmol) and pyridine (2.37g, 30 mmol) was added to the solution of toluene (20 mL) and naphthalene-1,4-diamine. The reaction mixture was stirred at 100 °C for 2 h under nitrogen. After cooling to room temperature, reaction mixture was then diluted in 20 mL of petroleum ether. After filtration, the solid was collected and washed with 1 M hydrochloric acid. Recrystallization from acetonitrile gave the gray solid, yield 67%; mp 252−254 °C. ^{1}H NMR (300 MHz, DMSO, δ) 10.10 (s, 2H), 7.98−7.95 (m, 2H), 7.53−7.50 (m, 4H), 7.41−7.39 (m, 2H), 7.29−7.26 (m, 4H), 6.99 (s, 2H), 2.32 (s, 6H). HRMS (ESI): found 489.0943 ($C_{24}H_{22}N_2NaO_4S_2$, $[M + NH_4]^+$, requires 489.0913).

*Diethyl 2,2′-(Naphthalene-1,4-diylbis(tosylazanediyl))diacetate (**17a**).* To a solution of **16a** (932 mg, 2 mmol) in DMF (5 mL) was added K_2CO_3 (830 mg, 6 mmol), followed by ethyl bromoacetate (836 mg, 5 mmol). After 3 h stirring at room temperature, the reaction mixture was then diluted in 30 mL of water and quenched with 2 M hydrochloric acid to pH 5. The crude product was obtained through filtration. Recrystallization from ethyl acetate/*n*-hexane gave the **17a** as a light-pink solid, yield 54%; mp 138−140 °C. ^{1}H NMR (300 MHz, DMSO, δ) 8.31−8.29 (m, 1H), 8.17−8.16 (m, 1H), 7.59−7.54 (m, 6H), 7.45−7.42 (m, 2H), 7.37−7.35 (m, 2H), 7.08 (s, 1H), 6.83 (s, 1H), 4.59−4.53 (m, 4H), 4.05−3.95 (m, 4H), 2.46(s, 3H), 2.39 (s, 3H), 1.10−1.03 (m, 6H). HRMS (ESI): found 656.2116 ($C_{32}H_{38}N_3O_8S_2$, $[M + NH_4]^+$, requires 656.2095).

*2,2′-(Naphthalene-1,4-diylbis(tosylazanediyl))diacetic Acid (**18a**).* To a solution of NaOH (2 g) in MeOH/H_2O (10/10 mL) was added **17a** (638 mg, 1 mmol). The reaction mixture was heated in an oil bath maintained at 65 °C for 2 h, then quenched with 2 M hydrochloric acid to pH 2 and diluted with 75 mL of water. Precipitate removed by filtration and washed with 5 × 10 mL water, then dried overnight in a vacuum desiccator, yielding **18a** as a white solid, yield 68%; mp 240−241 °C. ^{1}H NMR (300 MHz, DMSO, δ) 12.80 (br, 2H), 8.28−8.25 (m, 1H), 8.15−8.11 (m, 1H), 7.58−7.51 (m, 6H), 7.42−7.39 (m, 2H), 7.35−7.32 (m, 2H), 7.10 (s, 1H), 6.85 (s, 1H), 4.50−4.33 (m, 4H), 2.44 (s, 3H), 2.37 (s, 3H). ^{13}C NMR (75 MHz, DMSO, δ) 169.814, 143.775, 136.905, 135.046, 134.374, 132.915, 132.714, 129.580, 127.872, 127.611, 126.753, 126.659, 126.192, 124.656, 53.226, 53.010, 21.067, 21.001. HRMS (ESI): found 600.1480 ($C_{28}H_{30}N_3O_8S_2$, $[M + NH_4]^+$, requires 600.1469). HPLC (70:30 methanol:water with 1‰ TFA): t_R = 8.1 min, 99.5%.

*2,2′-(Naphthalene-1,4-diylbis(((4-fluorophenyl)sulfonyl)-azanediyl))diacetic Acid (**18b**).* The same procedure as **18a**, gray solid, yield 38%; mp 250−252 °C. ^{1}H NMR (300 MHz, DMSO, δ) 8.21−8.19 (m, 1H), 8.11−8.09 (m, 1H), 7.72−7.70 (m, 4H), 7.61−

DOI: 10.1021/acs.jmedchem.5b00185
J. Med. Chem. XXXX, XXX, XXX−XXX

7.50 (m, 2H), 7.46−7.32 (m, 4H), 7.17 (s, 1H), 7.02 (s, 1H), 4.53−4.37 (m, 4H). ^{13}C NMR (75 MHz, DMSO, δ) 169.919, 136.769, 134.430, 133.896, 132.773, 132.612, 131.011, 130.886, 130.758, 130.634, 130.086, 127.045, 126.688, 124.496, 116.385, 116.108, 53.419, 14.377. HRMS (ESI): found 608.0949 ($C_{26}H_{24}F_2N_3O_8S_2$, $[M + NH_4]^+$, requires 608.0967) HPLC (70:30 methanol:water with 1‰ TFA): t_R = 8.6 min, 95.2%.

*2,2′-(Naphthalene-1,4-diylbis(((4-chlorophenyl)sulfonyl)-azanediyl))diacetic Acid (**18c**).* The same procedure as **18a**, light-brown solid, yield 36%; mp 225−227 °C. ^{1}H NMR (300 MHz, DMSO, δ) 8.29−8.20 (m, 1H), 8.18−8.08 (m, 1H), 7.77−7.56 (m, 10H), 7.20 (s, 1H), 6.92 (s, 1H), 4.51−4.29 (m, 4H). ^{13}C NMR (75 MHz, DMSO, δ) 170.028, 138.099, 137.149, 136.675, 132.795, 129.809, 129.533, 127.007, 126.610, 124.536, 53.918. HRMS (ESI): found 640.0388 ($C_{26}H_{24}Cl_2N_3O_8S_2$, $[M + NH_4]^+$, requires 640.0376). HPLC (70:30 methanol:water with 1‰ TFA): t_R = 14.5 min, 95.8%.

*2,2′-(Naphthalene-1,4-diylbis(((4-bromophenyl)sulfonyl)-azanediyl))diacetic Acid (**18d**).* The same procedure as **18a**, light-brown solid, yield 42%; mp 243−244 °C. ^{1}H NMR (300 MHz, DMSO, δ) 8.24−8.23 (m, 1H), 8.22−8.18 (m, 1H), 7.77−7.72 (m, 4H), 7.62−7.60 (m, 4H), 7.53−7.52 (m, 2H), 7.29−7.18 (m, 1H), 6.95−6.87 (m, 1H), 4.31−4.19 (m, 2H), 4.03−3.97 (m, 2H). HRMS (ESI): found 727.9358 ($C_{26}H_2Br_2N_2NaO_8S_2$, $[M + NH_4]^+$, requires 727.9366). HPLC (70:30 methanol:water with 1‰ TFA): t_R = 8.7 min, 99.5%.

*2,2′-(Naphthalene-1,4-diylbis(((4-acetamidophenyl)sulfonyl)-azanediyl))diacetic Acid (**18e**).* The same procedure as **18a**, light-pink solid, yield 33%; mp 288−290 °C. ^{1}H NMR (300 MHz, DMSO, δ) 10.74 (s, 1H), 10.47 (s, 1H), 8.35 (dd, 1H, J = 6.23, 3.08 Hz), 8.18 (dd, 1H, J = 6.36, 3.06 Hz), 7.90 (d, 2H, J = 8.61 Hz), 7.74 (d, 2H, J = 8.73 Hz), 7.58−7.55 (m, 6H), 7.11 (s, 1H), 6.82 (s, 1H), 4.48−4.28 (m, 4H), 2.17(s, 3H), 2.09 (s, 3H). HRMS (ESI): found 686.1614 ($C_{30}H_{32}N_5O_{10}S_2$, $[M + NH_4]^+$, requires 686.1585). HPLC (70:30 methanol:water with 1‰ TFA): t_R = 3.3 min, 98.5%.

*2,2′-(Naphthalene-1,4-diylbis(((4-(tert-butyl)phenyl)sulfonyl)-azanediyl))diacetic Acid (**18f**).* The same procedure as **18a**, gray solid, yield 67%; mp 290−291 °C. ^{1}H NMR (300 MHz, DMSO, δ) 8.11−8.06 (m, 1H), 8.05−7.95 (m, 1H), 7.60−7.55 (m, 8H), 7.49−7.35 (m, 2H), 7.23 (s, 1H), 7.01(s, 1H), 4.33−4.13 (m, 4H), 1.33−1.28 (m, 18H). ^{13}C NMR (75 MHz, DMSO, δ) 170.129, 156.113, 136.863, 135.364, 132.771, 127.575, 127.372, 126.540, 126.099, 125.775, 124.489, 53.561, 34.843, 30.776. HRMS (ESI): found 689.1931 ($C_{34}H_{38}N_2NaO_8S_2$, $[M + Na]^+$, requires 689.1962). HPLC (70:30 methanol:water with 1‰ TFA): t_R = 9.2 min, 96.3%.

*2,2′-(Naphthalene-1,4-diylbis((mesitylsulfonyl)azanediyl))-diacetic Acid (**18g**).* The same procedure as **18a**, white solid, yield 61%; mp 116−118 °C. ^{1}H NMR (300 MHz, DMSO, δ) 7.87−7.84 (m, 2H), 7.58 (s, 1H), 7.51 (s, 1H), 7.40−7.37 (m, 2H), 6.96 (s, 2H), 6.89 (s, 2H), 4.70−4.64 (m, 2H), 4.34−4.28 (m, 2H), 2.25−2.16 (m, 18H). HRMS (ESI): found 656.2113 ($C_{32}H_{38}N_3O_8S_2$, $[M + NH_4]^+$, requires 656.2095). HPLC (70:30 methanol: water with 1‰ TFA): t_R = 7.0 min, 96.6%.

*2,2′-(Naphthalene-1,4-diylbis((phenylsulfonyl)azanediyl))diacetic Acid (**18h**).* The same procedure as **18a**, white solid, yield 44%; mp 265−266 °C. ^{1}H NMR (300 MHz, DMSO, δ) 12.90 (br, 2H), 8.25−8.22 (m, 1H), 8.10−8.07 (m, 1H), 7.77−7.51 (m, 12H), 7.15 (s, 1H), 6.90 (s, 1H), 4.57−4.36 (m, 4H). ^{13}C NMR (75 MHz, DMSO, δ) 169.818, 137.956, 137.297, 136.794, 133.468, 132.764, 132.584, 129.203, 129.142, 127.732, 127.512, 127.032, 126.644, 126.508, 124.500, 124.291, 53.185. HRMS (ESI): found 572.1133 ($C_{26}H_{26}N_3O_8S_2$, $[M + NH_4]^+$, requires 572.1156). HPLC (70:30 methanol:water with 1‰ TFA): t_R = 5.4 min, 98.1%.

*2,2′-(Naphthalene-1,4-diylbis(((4-(trifluoromethoxy)phenyl)-sulfonyl)azanediyl))diacetic Acid (**18i**).* To a solution of **17i** in methanol was added Pd/C. The reaction mixture was heated to 40 °C under hydrogen for 4 h. The solution was filtered to remove the catalyst. The filtrate was concentrated under reduced pressure to give the crude product. The crude product was washed by ether to give the gray solid, yield 68%; mp 291−293 °C. ^{1}H NMR (300 MHz, DMSO, δ) 12.91 (s, 2H), 8.16−8.14 (m, 1H), 8.04−8.01 (m, 1H), 7.81−7.77 (m, 4H), 7.57−7.50 (m, 6H), 7.29 (s, 1H), 7.01 (s, 1H), 4.64−4.35 (m, 4H). HRMS (ESI): found 740.0827 ($C_{28}H_{24}F_6N_3O_{10}S_2$, $[M + NH_4]^+$, requires 740.0802). HPLC (70:30 methanol:water with 1‰ TFA): t_R = 6.5 min, 97.1%.

*2,2′-(Naphthalene-1,4-diylbis((naphthalen-2-ylsulfonyl)-azanediyl))diacetic Acid (**18j**).* The same procedure as **18i**, gray solid, yield 68%; mp 243−245 °C. ^{1}H NMR (300 MHz, DMSO, δ) 8.38−8.33 (m, 3H), 8.19−7.93 (m, 7H), 7.79−7.48 (m, 6H), 7.47−7.46 (m, 2H), 7.12 (s, 1H), 6.78 (s, 1H), 4.46−4.33 (m, 4H). HRMS (ESI): found 677.1023 ($C_{34}H_{26}N_2NaO_8S_2$, $[M + Na]^+$, requires 677.1023). HPLC (70:30 methanol:water with 1‰ TFA): t_R = 17.1 min, 95.2%.

*2,2′-(Naphthalene-1,4-diylbis(((4-(trifluoromethyl)phenyl)-sulfonyl)azanediyl))diacetic Acid (**18k**).* The same procedure as **18i**, white solid, yield 44%; mp > 300 °C. ^{1}H NMR (300 MHz, DMSO, δ) 8.23−8.13 (m, 2H), 8.03−7.89 (m, 8H), 7.58−7.41 (m, 2H), 6.86 (s, 2H), 4.35−4.10 (m, 4H). HRMS (ESI): found 708.0916 ($C_{28}H_{24}F_6N_3O_8S_2$, $[M + NH_4]^+$, requires 708.0904). HPLC (70:30 methanol: water with 1‰ TFA): t_R = 6.3 min, 99.9%

*2,2′-(Naphthalene-1,4-diylbis(((3-methoxyphenyl)sulfonyl)-azanediyl))diacetic Acid (**18l**).* The same procedure as **18i**, white solid, yield 48%; mp 149−150 °C. ^{1}H NMR (300 MHz, DMSO, δ) 8.13 (s, 2H) 7.63−7.50 (m, 4H) 7.26−7.13 (m, 7H) 7.02 (s, 1H) 4.56−4.39 (m, 4H) 3.76 (s, 3H) 3.67 (s, 3H). ^{13}C NMR (75 MHz, DMSO, δ) 173.551, 164.125, 163.034, 143.636, 141.502, 137.348, 135.114, 134.995, 131.641, 131.389, 129.079,124.639, 124.502, 124.420, 116.871, 116.623, 60.266, 57.795, 35.380. HRMS (ESI): found 637.0931 ($C_{28}H_{26}N_2NaO_{10}S_2$, $[M + Na]^+$, requires 637.0921). HPLC (70:30 methanol:water with 1‰ TFA): t_R = 8.1 min, 96.2%

*2,2′-(Naphthalene-1,4-diylbis(((4-cyanophenyl)sulfonyl)-azanediyl))diacetic Acid (**18m**).* The same procedure as **12c**, gray solid, yield 69%; mp 265−267 °C. ^{1}H NMR (300 MHz, DMSO, δ) 12.95 (br, 2H), 8.22−7.96 (m, 6H), 7.87−7.71 (m, 4H), 7.57−7.55 (m, 2H), 7.18−7.10 (m, 2H), 4.60−4.35 (m, 4H). ^{13}C NMR (75 MHz, DMSO, δ) 169.743, 166.490, 166.125, 138.247, 136.729, 132.603, 130.022, 128.271, 127.885, 127.788, 127.600, 126.878, 124.385, 53.085. HRMS (ESI): found 627.0564 ($C_{28}H_{20}N_4NaO_8S_2$, $[M + Na]^+$, requires 627.0615). HPLC (70:30 methanol:water with 1‰ TFA): t_R = 3.6 min, 97.3%.

*2,2′-(Naphthalene-1,4-diylbis(((4-(tert-butyl)phenyl)sulfonyl)-azanediyl))diacetic Acid (**18n**).* The same procedure as for **18i**, white solid, yield 62%; mp 222−224 °C. ^{1}H NMR (300 MHz, DMSO, δ) 11.82 (s, 2H), 8.32−8.30 (m, 1H), 8.19−8.17 (m, 1H), 7.56−7.53 (m, 6H), 7.12−7.02 (m, 5H), 6.85 (s, 1H), 4.46−4.30 (m, 4H), 4.19−4.05 (m, 4H), 1.80−1.67 (m, 4H), 1.51−1.46 (m, 4H), 0.99−0.94 (m, 6H). HRMS (ESI): found 682.6418 ($C_{34}H_{42}N_3O_8S_2$, $[M + NH_4]^+$, requires 682.2408). HPLC (70:30 methanol:water with 1‰ TFA): t_R = 7.2 min, 96.8%.

*2,2′-(Naphthalene-1,5-diylbis(((4-methoxyphenyl)sulfonyl)-azanediyl))diacetic Acid (**15**).* **15** was synthesized according to the procedure of **18m**, gray solid, yield 71%; mp 267−269 °C. ^{1}H NMR (300 MHz, DMSO, δ) 12.82 (s, 2H), 8.29−8.26 (m, 2H), 7.61−7.57 (m, 4H), 7.46−7.34 (m, 2H), 7.22−6.98 (m, 6H), 4.42−4.39 (m, 4H) 3.87 (s, 3H) 3.85 (s, 3H). ^{13}C NMR (75 MHz, DMSO, δ) 169.989, 169.884, 162.826, 136.680, 133.135, 129.937, 129.281, 127.376, 125.648, 114.304, 55.668, 53.294. HRMS (ESI): found 632.1349 ($C_{28}H_{30}N_3O_{10}S_2$, $[M + NH_4]^+$, requires 632.1367). HPLC (70:30 methanol:water with 1‰ TFA): t_R = 5.6 min, 97.2%.

2. Molecular Docking. The Ligandfit docking tool in Discovery Studio, which has been validated for this target previously,[14,16] was used to predict the binding mode of the small molecular inhibitor. The docking site was derived from the position of the small molecular ligand cocrystallized in the binding site of Keap1 (PDB code 4IQK).

3. Physicochemical Properties. The pK_a and partition coefficient (log D, pH 7.4) were determined according to the methods of Avdeef and Tsinman[23] on a Gemini Profiler instrument (pION) by the "gold standard" Avdeef−Bucher potentiometric titration method.[24] The experimental procedures were carried out as previously reported.[25] The pH-metric method was used to determine the intrinsic solubility. This is a new potentiometric acid−base titration method. The potentiometric solubility data were obtained with the pSOL model 3

DOI: 10.1021/acs.jmedchem.5b00185
J. Med. Chem. XXXX, XXX, XXX−XXX

instrument (pION INC., Cambridge, MA, USA) and subsequently processed with the accompanying computer program, pS. The detailed mechanism and experimental procedures can be found in the refs 26−28.

4. Biology. *4.1. FP Competition Assays to Determine the Inhibitory Potency of the Keap1−Nrf2 Interaction.* Generally, the FP assay was carried out as previously reported.[16] The experiments were performed on a SpectraMax multimode microplate reader (Molecular Devices) using the excitation and emission filters appropriate for the FITC. The plates used for the FP measurements were black nonbinding surface Corning 3676 384-well plates, loaded with 40 μL of assay solution per well, consisting of 10 μL of 4 nM FITC-9mer Nrf2 peptide amide and 10 μL of 12 nM Keap1 Kelch domain protein, 10 μL of HEPES buffer, and 10 μL of an inhibitor sample of varying concentrations. The plate was covered and rocked for 30 min at room temperature prior to FP measurements. FP was determined by measuring the parallel and perpendicular fluorescence intensity ($F\|$ and $F\perp$) with respect to the linearly polarized excitation light. We elected to use polarization in our quantitative analysis. The percentage inhibition of the competitor at each concentration point was determined by using the equation %inhibition = $1 - (P_{obs} - P_{min})/(P_{max} - P_{min})$. The values of P_{max}, P_{min}, and P_{obs} in the equations refer to the polarization of the wells containing Keap1 and the probe, the polarization of the free probe, and the observed polarization for the wells containing the inhibitors at a range of concentrations under the assay conditions, respectively. The IC_{50} of an inhibitor was determined from the plot of %inhibition against inhibitor concentration as analyzed by GraphPad Prism 6.0 software.

4.2. Cell Culture Conditions and ARE-Luciferase Activity Assay. HepG2 cells stably transfected with a luciferase reporter (HepG2−ARE−C8) were kindly provided by Professor Dr. A. N. Tony Kong (Rutgers University, Piscataway, NJ) and Prof. Rong Hu (China Pharmaceutical University, Nanjing). The cells were maintained in modified RPMI-1640 medium (GiBco, Invitrogen Corp., USA) with 10% fetal bovine serum (FBS) (Gibco, Invitrogen Corp., USA) in a humidified atmosphere of 5% CO_2 and 95% air at 37 °C. HCT116 cells (Cell Bank of Shanghai Institute of Biochemistry and Cell Biology, Shanghai Institutes for Biological Sciences, Chinese Academy of Sciences) were cultured in McCoy's 5A medium (Sigma-Aldrich, no. M4892, USA) supplemented with 10% (v/v) FBS.

The experimental procedures were carried out as reported previously.[16,24] Generally, HepG2−ARE−C8 cells were plated in 96-well plates at a density of 4×10^4 cells/well and incubated overnight. The cells were exposed to different concentrations of test compounds, with **8** serving as a positive control, DMSO as a negative control, and the luciferase cell culture lysis reagent as a blank. After 12 h of treatment, the medium was removed and 100 μL of cold PBS was added to each well. Then, the cells were harvested in the luciferase cell culture lysis reagent. After centrifugation, 20 μL of the supernatant was used to determine the luciferase activity according to the protocol provided by the manufacturer (Promega, Madison, WI). The luciferase activity was measured by a Luminoskan Ascent (Thermo Scientific, USA). The data were obtained in triplicate and expressed as fold induction over the control. Induction fold = $(RLU_{test} - RLU_{blank})/(RLU_{DMSO\ control} - RLU_{blank})$. RLU = relative light unit.

4.3. Western Blotting. Anti-NQO1 (sc-271116) antibodies and γ-GCS (sc-22755) antibodies were from Santa Cruz Biotechnology (Santa Cruz, CA, USA). Anti-β-actin (AP0060) and anti-Nrf2 (BS1258) were purchased from Bioworlde (Bioworlde, USA). Anti-HO-1 (no. 5853S) was purchased from Cell Signaling Technology (USA). The cells were washed once with ice-cold PBS and driven down with 1 mL of 1× pancreatic enzymes. The cells were centrifuged at 2500 rpm and resuspended in 45.0 μL of lysis buffer, which was composed of 50.0 mM Tris-HCl, 150.0 mM NaCl, NP-40, 1 mM EDTA, PMSF, NaF, Leu, and DTT for 1 h. Then, cells were centrifuged again at 12000 rpm for 20 min at 4 °C. The supernatant was retained, and the protein concentration was determined by the BCA assay with Varioskan flash (Thermo, Waltham, MA) at 562 nm. The samples were stored at −80 °C until use. The extracts were separated by SDS-PAGE and then transferred onto PVDF membranes (PerkinElmer, Northwalk, CT, USA). After blocking with 1% BSA for 2 h, the membranes were incubated at 37 °C for 1 h and then at 4 °C overnight with a primary antibody. After that, they were reacted with a DyLight 800 labeled secondary antibody at 37 °C for 1 h. The membranes were screened through the Odyssey infrared imaging system (LI-COR, Lincoln, Nebraska, USA).

4.4. RNA Extraction and qRT-PCR Analysis. Total RNA of HCT116 cells was isolated using TRIzol (Invitrogen). The quantification and purity of RNA samples was assessed by A260/A280 absorption, and RNA samples with ratios above 1.8 were stored at −80 °C for further analysis. The RNA was reverse transcribed by the PrimeScrpt RT reagent kit following the manufacturer's instructions. The sequence of primers used for PCR can be found in the Supporting Information. Quantitative real-time RT-PCR analysis of Nrf2, NQO1, HO-1, and GCLM was performed by using the StepOne System Fast Real Time PCR system (Applied Biosystems). The values are expressed as the fold change from the control. β-Actin was used for normalization. Each cycle consisted of denaturation at 95 °C for 5 s and combined annealing and extension at 60 °C for 30 s. A total of 55 cycles was performed.

4.4. Transfection of Small Interfering RNA (siRNA). Predesigned siRNA against human Nrf2 (catalogue no. 115762) and control scrambled siRNA (catalogue no. 4611) were purchased from Biomics (Biomics, China). HCT116 cells were plated at a density of 7×10^5 cells per 60 mm dish. The cells were transfected with 50 nM siRNA against Nrf2 or 50.0 nM scrambled duplex using Lipofectamine 2000 (Invitrogen). After a 24 h incubation, fresh medium was added, and the cells were cultured for another 48 h. The cells were then treated with 20.0 μM compound **18e** for an additional 6 h and lysed for use in qRT-PCR.

4.5. LPS Challenge Mouse Acute Inflammation Model. Animal studies were conducted according to protocols approved by Institutional Animal Care and Use Committee of China Pharmaceutical University. All animals were appropriately used in a scientifically valid and ethical manner. Female C57BL/6 mice (12−16 weeks) were randomly divided into five groups (n = 10): control group, dexamethasone (Sigma-Aldrich, St. Louis, no. D4902) group (10 mg/kg/day), LPS (Sigma-Aldrich, St. Louis, no. L4130) group (300 μg/kg/day), compound **18e** low-dose (10 mg/kg/day) group, and compound **18e** high-dose (80 mg/kg/day) group. The **18e** and dexamethasone pretreated animals received a single IP injection (500.0 μL) containing the desired dose (day −3, −2, −1). All LPS-challenged mice (blank control, dexamethasone pretreated, **18e** pretreated) received 300.0 μg IP LPS 24 h after the last dose of dexamethasone or **18e** (day 0). Organs and sera were collected 5 h after the LPS challenge on day 0. Individual serum samples (n = 10) were placed immediately on ice after collection and were centrifuged at 12000g before plasma was obtained and frozen at −20 °C for ELISA. Plasma was assayed for murine IL-6 (EK0411, IL-6 (m) ELISA kit 1200, Boster, China), TNF-α (EK0527, TNFα (m) ELISA kit 1200, Boster, China), IFN-γ (EK0375, IFNγ (m) ELISA kit 1000, Boster, China), IL-17 (EK0431, IL-17 (m) ELISA kit 1200, Boster, China), and IL-12 (EK0422, IL-12 (P70) (m) ELISA kit 1200, Boster, China) using double-sandwich ELISA techniques.

■ ASSOCIATED CONTENT

Supporting Information

The Supporting Information is available free of charge on the ACS Publications website at DOI: 10.1021/acs.jmedchem.5b00185.

Characterization of the other intermediates, detailed results of SPR study, binding mode predication of **15**, mice body weight records of the in vivo experiments, and sequences used for PCR (PDF)

DOI: 10.1021/acs.jmedchem.5b00185
J. Med. Chem. XXXX, XXX, XXX−XXX

AUTHOR INFORMATION

Corresponding Authors

*For H.-P.S.: Phone/Fax: +86 025 83271216. E-mail: sunhaopeng@163.com.

*For Q.-D.Y.: Phone/Fax: +86 025 83271351. E-mail: youqidong@gmail.com.

Author Contributions

The manuscript was written through contributions of all authors. All authors have given approval to the final version of the manuscript.

Notes

The authors declare no competing financial interest.

ACKNOWLEDGMENTS

This work is supported by the projects 81230078 (key program), 81202463 (youth foundation), 81173087 and 91129732 of National Natural Science Foundation of China, 2014ZX09507002-005-015, 2013ZX09402102-001-005, and 2010ZX09401-401 of the National Major Science and Technology Project of China (Innovation and Development of New Drugs), and Specialized Research Fund for the Doctoral Program of Higher Education (SRFDP, 20130096110002). HepG2 cells stably transfected with a luciferase reporter (HepG2-ARE-C8) were kindly provided by Professor Dr. A. N. Tony Kong (Rutgers University, Piscataway, NJ) and Prof. Rong Hu (China Pharmaceutical University, Nanjing).

ABBREVIATIONS USED

Keap1, Kelch-like ECH-associated protein-1; Nrf2, nuclear factor erythroid 2-related factor 2; LPS, lipopolysaccharide; bZIP, basic leucine zipper; TAT, trans-activating transcriptional; ARE, antioxidant response element; PPI, protein−protein interaction; NQO1, NAD(P)H/quinone oxidoreductase; HO-1, heme oxygenase-1; GCLM, glutamate−cysteine ligase modifier subunit; GCS, glutamylcysteine synthetase

REFERENCES

(1) Kobayashi, M.; Yamamoto, M. Molecular mechanisms activating the Nrf2-Keap1 pathway of antioxidant gene regulation. *Antioxid. Redox Signaling* **2005**, *7*, 385−94.

(2) Stepkowski, T. M.; Kruszewski, M. K. Molecular cross-talk between the NRF2/KEAP1 signaling pathway, autophagy, and apoptosis. *Free Radical Biol. Med.* **2011**, *50*, 1186−95.

(3) Taguchi, K.; Motohashi, H.; Yamamoto, M. Molecular mechanisms of the Keap1−Nrf2 pathway in stress response and cancer evolution. *Genes to Cells* **2011**, *16*, 123−140.

(4) Wilson, A. J.; Kerns, J. K.; Callahan, J. F.; Moody, C. J. Keap calm, and carry on covalently. *J. Med. Chem.* **2013**, *56*, 7463−76.

(5) Magesh, S.; Chen, Y.; Hu, L. Small Molecule Modulators of Keap1−Nrf2-ARE Pathway as Potential Preventive and Therapeutic Agents. *Med. Res. Rev.* **2012**, *32*, 687−726.

(6) Suzuki, T.; Motohashi, H.; Yamamoto, M. Toward clinical application of the Keap1−Nrf2 pathway. *Trends Pharmacol. Sci.* **2013**, *34*, 340−346.

(7) Cleasby, A.; Yon, J.; Day, P. J.; Richardson, C.; Tickle, I. J.; Williams, P. A.; Callahan, J. F.; Carr, R.; Concha, N.; Kerns, J. K.; Qi, H.; Sweitzer, T.; Ward, P.; Davies, T. G. Structure of the BTB Domain of Keap1 and Its Interaction with the Triterpenoid Antagonist CDDO. *PLoS One* **2014**, *9*, e98896.

(8) Hancock, R.; Bertrand, H. C.; Tsujita, T.; Naz, S.; El-Bakry, A.; Laoruchupong, J.; Hayes, J. D.; Wells, G. Peptide inhibitors of the Keap1−Nrf2 protein-protein interaction. *Free Radical Biol. Med.* **2012**, *52*, 444−51.

(9) Steel, R.; Cowan, J.; Payerne, E.; O'Connell, M. A.; Searcey, M. Anti-inflammatory Effect of a Cell-Penetrating Peptide Targeting the Nrf2/Keap1 Interaction. *ACS Med. Chem. Lett.* **2012**, *3*, 407−410.

(10) Bowman, A. L.; Nikolovska-Coleska, Z.; Zhong, H.; Wang, S.; Carlson, H. A. Small molecule inhibitors of the MDM2-p53 interaction discovered by ensemble-based receptor models. *J. Am. Chem. Soc.* **2007**, *129*, 12809−14.

(11) Hu, L.; Magesh, S.; Chen, L.; Wang, L.; Lewis, T. A.; Chen, Y.; Khodier, C.; Inoyama, D.; Beamer, L. J.; Emge, T. J.; Shen, J.; Kerrigan, J. E.; Kong, A. N.; Dandapani, S.; Palmer, M.; Schreiber, S. L.; Munoz, B. Discovery of a small-molecule inhibitor and cellular probe of Keap1−Nrf2 protein-protein interaction. *Bioorg. Med. Chem. Lett.* **2013**, *23*, 3039−43.

(12) Jnoff, E.; Albrecht, C.; Barker, J. J.; Barker, O.; Beaumont, E.; Bromidge, S.; Brookfield, F.; Brooks, M.; Bubert, C.; Ceska, T.; Corden, V.; Dawson, G.; Duclos, S.; Fryatt, T.; Genicot, C.; Jigorel, E.; Kwong, J.; Maghames, R.; Mushi, I.; Pike, R.; Sands, Z. A.; Smith, M. A.; Stimson, C. C.; Courade, J. P. Binding mode and structure-activity relationships around direct inhibitors of the Nrf2-Keap1 complex. *ChemMedChem* **2014**, *9*, 699−705.

(13) Marcotte, D.; Zeng, W.; Hus, J.-C.; McKenzie, A.; Hession, C.; Jin, P.; Bergeron, C.; Lugovskoy, A.; Enyedy, I.; Cuervo, H.; Wang, D.; Atmanene, C.; Roecklin, D.; Vecchi, M.; Vivat, V.; Kraemer, J.; Winkler, D.; Hong, V.; Chao, J.; Lukashev, M.; Silvian, L. Small molecules inhibit the interaction of Nrf2 and the Keap1 Kelch domain through a non-covalent mechanism. *Bioorg. Med. Chem.* **2013**, *21*, 4011−4019.

(14) Sun, H.-P.; Jiang, Z.-Y.; Zhang, M.-Y.; Lu, M.-C.; Yang, T.-T.; Pan, Y.; Huang, H.-Z.; Zhang, X.-J.; You, Q.-d. Novel protein-protein interaction inhibitor of Nrf2-Keap1 discovered by structure-based virtual screening. *MedChemComm* **2014**, *5*, 93−98.

(15) Zhuang, C.; Narayanapillai, S.; Zhang, W.; Sham, Y. Y.; Xing, C. Rapid identification of Keap1−Nrf2 small-molecule inhibitors through structure-based virtual screening and hit-based substructure search. *J. Med. Chem.* **2014**, *57*, 1121−6.

(16) Jiang, Z.-Y.; Lu, M.-C.; Xu, L. L.; Yang, T.-T.; Xi, M.-Y.; Xu, X.-L.; Guo, X.-K.; Zhang, X.-J.; You, Q.-D.; Sun, H.-P. Discovery of Potent Keap1−Nrf2 Protein−Protein Interaction Inhibitor Based on Molecular Binding Determinants Analysis. *J. Med. Chem.* **2014**, *57*, 2736−2745.

(17) Jiang, Z.-Y.; Xu, L.-L.; Lu, M.-C.; Pan, Y.; Huang, H.-Z.; Zhang, X.-J.; Sun, H.-P.; You, Q.-D. Investigation of the intermolecular recognition mechanism between the E3 ubiquitin ligase Keap1 and substrate based on multiple substrates analysis. *J. Comput.-Aided Mol. Des.* **2014**, *28*, 1233−1245.

(18) Shultz, M. D. Setting expectations in molecular optimizations: Strengths and limitations of commonly used composite parameters. *Bioorg. Med. Chem. Lett.* **2013**, *23* (21), 5980−91.

(19) Rushworth, S. A.; MacEwan, D. J.; O'Connell, M. A. Lipopolysaccharide-Induced Expression of NAD(P)H:Quinone Oxidoreductase 1 and Heme Oxygenase-1 Protects against Excessive Inflammatory Responses in Human Monocytes. *J. Immunol.* **2008**, *181*, 6730−6737.

(20) Akira, S.; Takeda, K. Toll-like receptor signalling. *Nat. Rev. Immunol.* **2004**, *4*, 499−511.

(21) Asehnoune, K.; Strassheim, D.; Mitra, S.; Kim, J. Y.; Abraham, E. Involvement of reactive oxygen species in Toll-like receptor 4-dependent activation of NF-kappa B. *J. Immunol.* **2004**, *172*, 2522−9.

(22) Auletta, J. J.; Alabran, J. L.; Kim, B. G.; Meyer, C. J.; Letterio, J. J. The synthetic triterpenoid, CDDO-Me, modulates the proinflammatory response to in vivo lipopolysaccharide challenge. *J. Interferon Cytokine Res.* **2010**, *30*, 497−508.

(23) Avdeef, A.; Tsinman, O. Miniaturized Rotating Disk Intrinsic Dissolution Rate Measurement: Effects of Buffer Capacity in Comparisons to Traditional Wood's Apparatus. *Pharm. Res.* **2008**, *25*, 2613−2627.

(24) Avdeef, A.; Bucher, J. J. Accurate measurements of the concentration of hydrogen ions with a glass electrode: calibrations using the Prideaux and other universal buffer solutions and a

DOI: 10.1021/acs.jmedchem.5b00185
J. Med. Chem. XXXX, XXX, XXX−XXX

computer-controlled automatic titrator. *Anal. Chem.* **1978**, *50*, 2137−2142.
(25) Zhang, X.; Li, X.; Sun, H.; Wang, X.; Zhao, L.; Gao, Y.; Liu, X.; Zhang, S.; Wang, Y.; Yang, Y.; Zeng, S.; Guo, Q.; You, Q. Garcinia Xanthones as Orally Active Antitumor Agents. *J. Med. Chem.* **2013**, *56*, 276−292.
(26) Avdeef, A.; Berger, C. M. pH-metric solubility.: 3. Dissolution titration template method for solubility determination. *Eur. J. Pharm. Sci.* **2001**, *14*, 281−291.
(27) Avdeef, A. pH-metric Solubility. 1. Solubility-pH Profiles from Bjerrum Plots. Gibbs Buffer and pKa in the Solid State. *Pharm. Pharmacol. Commun.* **1998**, *4*, 165−178.
(28) Xi, M. Y.; Jia, J. M.; Sun, H. P.; Sun, Z. Y.; Jiang, J. W.; Wang, Y. J.; Zhang, M. Y.; Zhu, J. F.; Xu, L. L.; Jiang, Z. Y.; Xue, X.; Ye, M.; Yang, X.; Gao, Y.; Tao, L.; Guo, X. K.; Xu, X. L.; Guo, Q. L.; Zhang, X. J.; Hu, R.; You, Q. D. 3-Aroylmethylene-2,3,6,7-tetrahydro-1H-pyrazino[2,1-a]isoquinolin-4(11bH)-ones as Potent Nrf2/ARE Inducers in Human Cancer Cells and AOM-DSS Treated Mice. *J. Med. Chem.* **2013**, *56*, 7925−7938.

DOI: 10.1021/acs.jmedchem.5b00185
J. Med. Chem. XXXX, XXX, XXX−XXX